Supporting Information

Tuning the surface properties of CuO films using the precursor ageing approach for enhanced photoelectrocatalytic reactions

Pannan I. Kyesmen[1], Nolwazi Nombona[2] and Mmantsae Diale[1*]*

Pannan I. Kyesmen, Mmantsae Diale

Department of Physics, University of Pretoria, Private Bag X20, Hatfield 0028, South Africa. E-mails: pannan.kyesmen@up.ac.za, mmantsae.diale@up.ac.za

Nolwazi Nombona

Department of Chemistry, University of Pretoria, Private Bag X20, Hatfield 0028, South Africa.

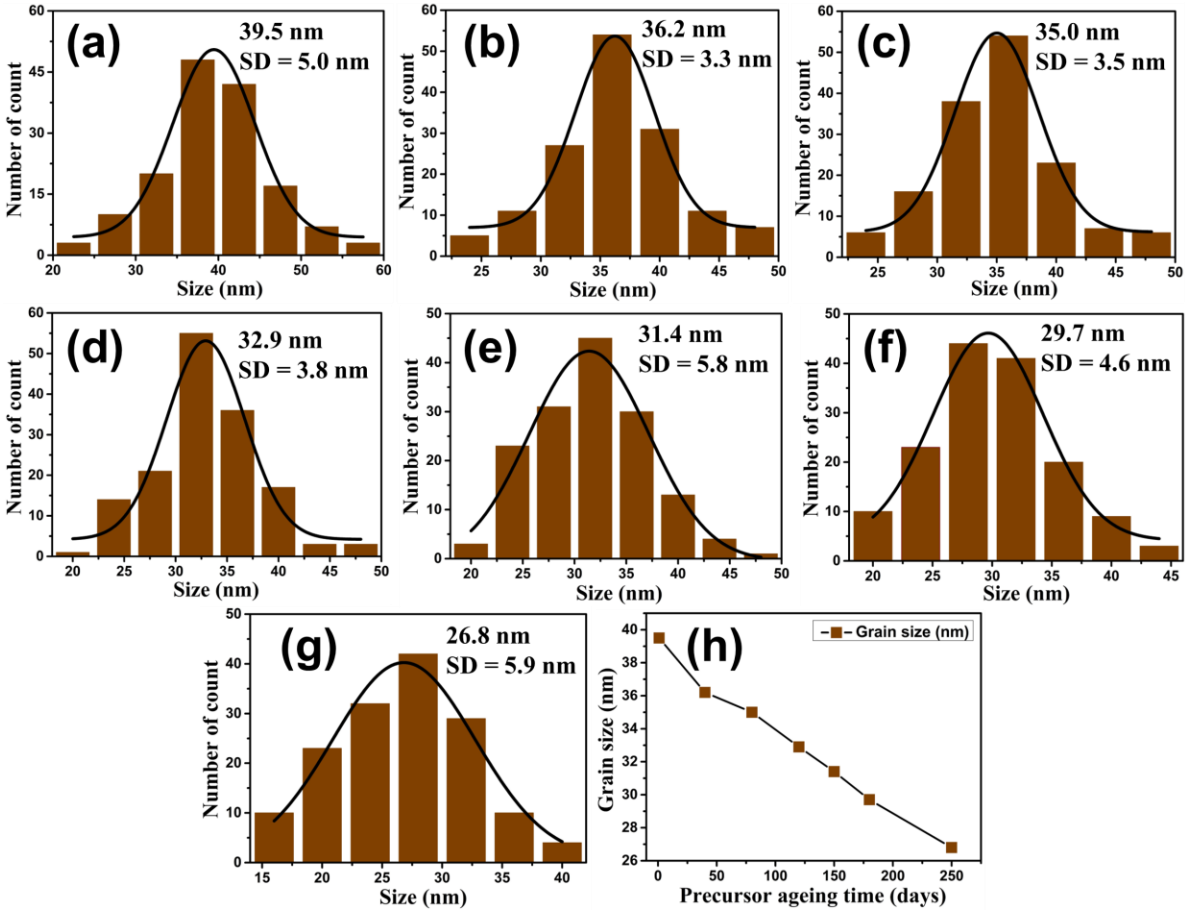

Figure S1. The histogram for the average particle diameter distribution for (a) CuO-1d, (b) CuO-40d, (c) CuO-80d, (d) CuO-120d, (e) CuO-150d, (f) CuO-180d, and (g) CuO-250d films respectively: (h) presents a plot of the grain size estimated for the films prepared using precursor solutions that were aged for 1-250 days.

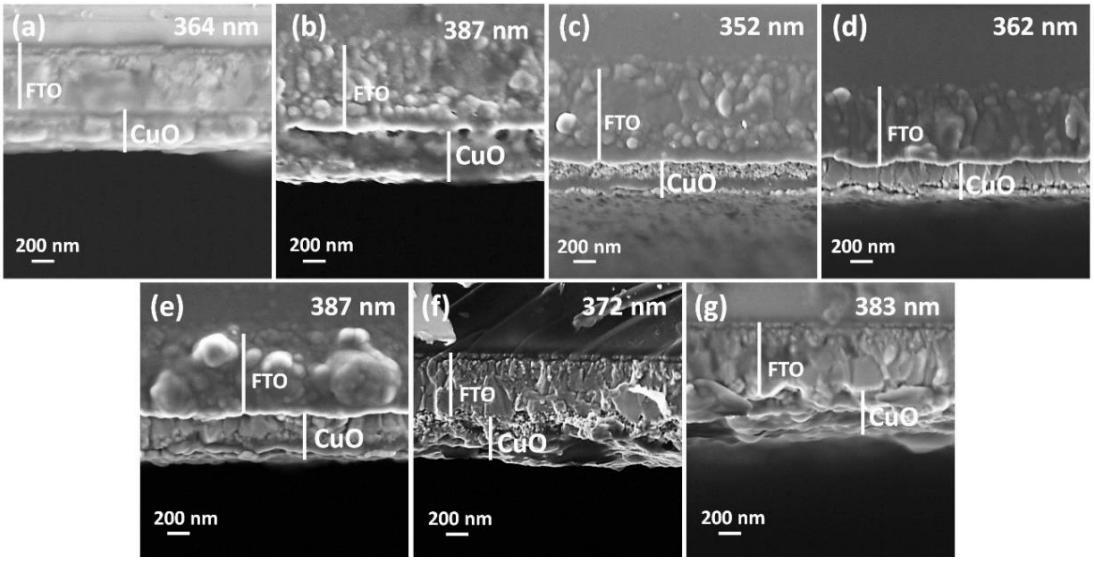

Figure S2. The cross-sectional image of (a) CuO-1d, (b) CuO-40d, (c) CuO-80d, (d) CuO-120d, (e) CuO-150d, (f) CuO-180d, and (g) CuO-250d samples.

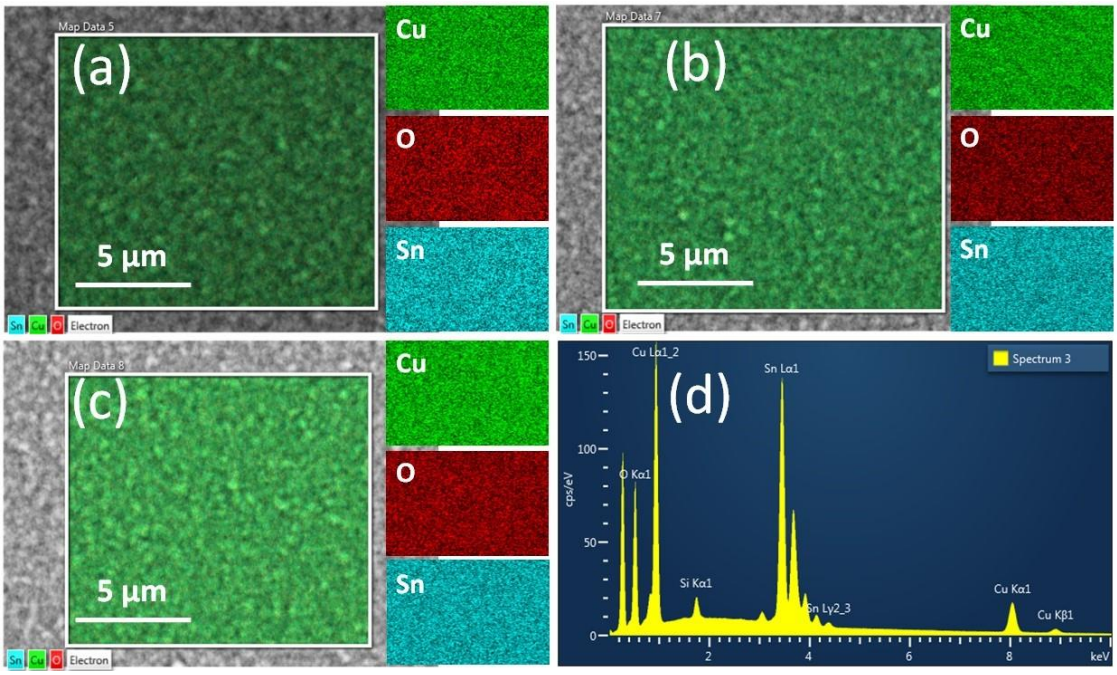

Figure S3. The EDS elemental distribution for (a) CuO-40d, (b) CuO-80d, and (c) CuO-120d samples: (d) shows the composition of the CuO-180d films after an EDS point scan.

Table S1. Direct and indirect bandgap values of dip-coated CuO films prepared using a precursor solutions that were aged for 1 to 250 days.

Sample	**Indirect Bandgap (eV)**	**direct Bandgap (eV)**
CuO-1d	1.34	2.29
CuO-40d	1.35	2.41
CuO-80d	1.31	2.32
CuO-120d	1.34	2.34
CuO-150d	1.27	2.27
CuO-180d	1.2	2.1
CuO-250d	1.21	2.14

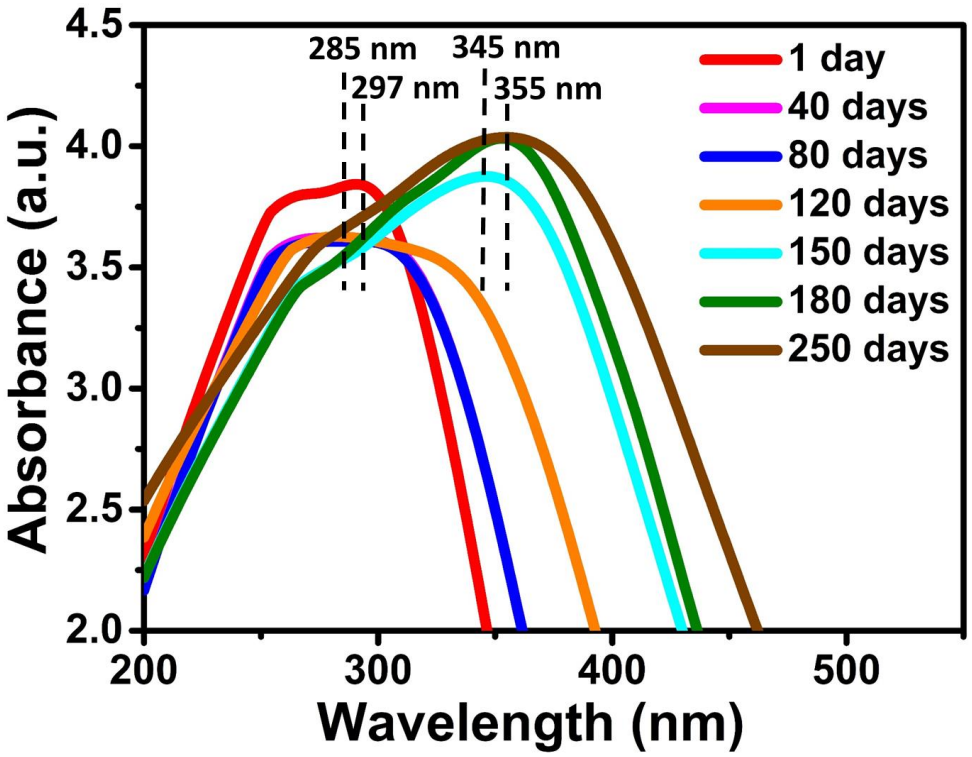

Figure S4. A magnified UV-Vis absorption spectra of copper-based solution that was aged for 1 to 250 days in the region of 200-550 nm, showing the red-shifting of the absorption peaks with precursor ageing.

Table S2. MS analysis data of dip-coated CuO photocathodes prepared using precursor solution that was aged for 1-250 days.

Sample	**N_A * 10^{20} (cm^{-3})**	**V_{fb} vs RHE (V) in 0.5M Na_2SO_4**	**E_{VB} (eV)**	**E_{CB} (eV)**
CuO-1d	3.3	0.678	0.88	-0.46
CuO-40d	6.9	0.670	0.87	-0.48
CuO-80d	6.0	0.652	0.85	-0.46
CuO-120d	2.8	0.696	0.90	-0.44
CuO-150d	2.1	0.729	0.93	-0.34

CuO-180	8.3	0.708	0.91	-0.29
CuO-250d	2.1	0.703	0.90	-0.31

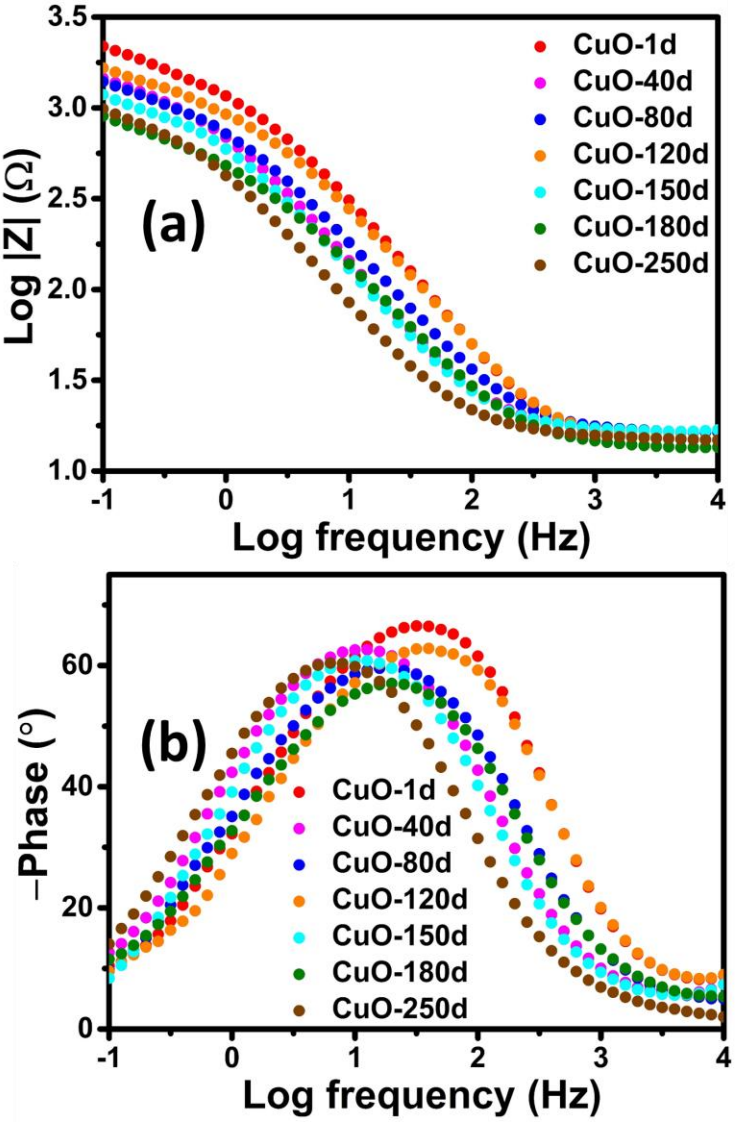

Figure S5. EIS (a) Bode plots of log |Z| vs log frequency, and (b) phase vs log frequency.

Bode plots obtained for the CuO photocathodes were analyzed to further examine the charge transport properties of the samples. The graphs of log |Z| against log frequency are given in Figure S5 (a) for all the photocathodes. The plot revealed the minimum log |Z| magnitude for CuO-180d samples and the highest value for CuO-1d films. A reduction in the Log |Z| value

indicates the reduction of resistance to charge transfer at the photoelectrode/liquid junction, which is essential in enhancing the catalytic response of photoelectrodes. The plots of phase angle vs log frequency are shown in Figure S5 (b) for all the CuO samples. The plots revealed the most positive peak for CuO-180d photocathodes. A more positive phase angle peak portrays evidence of a boost in charge carrier mobility at the electrode/electrolyte interface.[1]

Table S3. A comparison of the photocurrent density (J) achieved for the CuO photocathodes in this project with other reports in literature.

CuO films morphology	**Preparation method**	**Photocurrent density (J)**	**Reference**
CuO nanaparticles	Sol-gel dip coating	-1.6 mA/cm^2 at 0.35 V vs RHE, 1 M NaOH electrolyte, and under 1 sun.	This work
CuO Nanoparticles	Electrodeposition	-0.49 µA/cm^2 at -0.55 V vs Ag/AgCl, 1 M KOH electrolyte, 1 sun	[2]
CuO Nanoparticles	Thermal condensation	-0.50 mA/cm^2 at 0 V vs RHE, 0.1 M Na_2SO_4 electrolyte, and under 1 sun.	[3]
intermingled nanosheets	Microwave-assisted	-1.15 mA/cm2 at 0 V vs RHE, 0.1 M Na2SO4 electrolyte, and under 1 sun.	[4]
Nanoparticles	Electrodeposition	-1.39 mA/cm2 at 0 V vs RHE, 0.1 M Na2SO4 electrolyte, and under 1 sun	[5]
Nanoleaves	Sol-gel spin-coating	-0.3 mA/cm2 at -0.55 V vs SCE, 1 M NaOH electrolyte, and under 1 sun	[6]
Nanoparticles	Electrodeposition	-1.1 mA/cm2 at 0.1 V vs RHE, 0.2 M Na2SO4 electrolyte, and under 1 sun	[7]
Nanoleaves	Aqueous solution-based	-1.5 mA/cm2 at -0.6 V vs Ag/AgCl, 0.1 M Na2SO4 electrolyte, and under 1 sun	[8]
Nanorods	Sol-gel spin-coating	-1.13 mA/cm2 at -0.6 V vs SCE, 1 M KOH electrolyte, and under 1 sun	[9]
Nanosheets	Sol-gel spin-coating	-3.09 mA/cm2 at -0.5 V vs RHE, 0.5 M Na2SO4 electrolyte, and under 1 sun	[10]
Nanoparticles	Sputtering	-1.68 mA/cm2 at 0 V vs RHE, 0.1 M Na2SO4 electrolyte, and under 1 sun.	[11]
hollow spheres	doctor-blade	-1.47 mA/cm2 at -0.3 V vs Ag/AgCl, 0.5 M Na_2SO_4 electrolyte, and under 1 sun	[12]

References

[1] A. Mahmood, F. Tezcan, G. Kardaş, *International Journal of Hydrogen Energy* **2017**, 42, 23268.

[2] H. Xing, E. Lei, Z. Guo, D. Zhao, Z. Liu, *Chemical Engineering Journal* **2020**, 394, 124907.

[3] H. Bae, V. Burungale, W. Na, H. Rho, S. H. Kang, S.-W. Ryu, J.-S. Ha, *RSC advances* **2021**, 11, 16083.

[4] S. M. Hosseini H, R. Siavash Moakhar, F. Soleimani, S. K. S. Sadrnezhaad, presented at *Electrochemical Society Meeting Abstracts 237*, **2020**.

[5] Q. Zhang, B. Zhai, Z. Lin, X. Zhao, P. Diao, *International Journal of Hydrogen Energy* **2021**, 46, 11607.

[6] E. Mustafa, E. Dawi, Z. Ibupoto, A. Ibrahim, A. Elsukova, X. Liu, A. Tahira, R. Adam, M. Willander, O. Nur, *RSC advances* **2023**, 13, 11297.

[7] C.-J. Chang, C.-W. Lai, W.-C. Jiang, Y.-S. Li, C. Choi, H.-C. Yu, S.-J. Chen, Y. Choi, *Coatings* **2022**, 12, 1206.

[8] A. Kushwaha, R. S. Moakhar, G. K. Goh, G. K. Dalapati, *Journal of Photochemistry and Photobiology A: Chemistry* **2017**, 337, 54.

[9] S. Lee, Y. Hong, H. Ryu, J. Yun, *Thin Solid Films* **2020**, 697, 137849.

[10] M. Basu, *ChemPhotoChem* **2019**, 3, 1254.

[11] S. Masudy-Panah, R. S. Moakhar, C. S. Chua, A. Kushwaha, T. I. Wong, G. K. Dalapati, *RSC advances* **2016**, 6, 29383.

[12] Y.-H. Choi, D.-H. Kim, H. S. Han, S. Shin, S.-H. Hong, K. S. Hong, *Langmuir* **2014**, 30, 700.